Article

Integrated Network Pharmacology Analysis and Serum Metabolomics to Reveal the Anti-malaria Mechanism of Artesunate

Feiran Wang,[||] Jian Song,[||] Yingying Yan, Qian Zhou, Xiaojing Li, Ping Wang, Zongtong Yang, Qiuhong Zhang,* and Huimin Zhang*

ACCESS | Metrics & More | Article Recommendations

ABSTRACT: Artesunate is a widely used drug in clinical treatment of malaria. The aim of this study was to investigate the therapeutic mechanism of artesunate on malaria using an integrated strategy of network pharmacology and serum metabolomics. The mice models of malaria were established using 2×10^7 red blood cells infected with *Plasmodium berghei* ANKA injection. Giemsa and hematoxylin-eosin (HE) staining were used to evaluate the efficacy of artesunate on malaria. Next, network pharmacology analysis was applied to identify target genes. Then, a metabolomics strategy has been developed to find the possible significant serum metabolites and metabolic pathways induced by artesunate. Additionally, two parts of the results were integrated to confirm each other. Giemsa and HE staining results showed that artesunate significantly inhibited the proliferation of *Plasmodium* and reduced liver and spleen inflammation. Based on metabolomics, 18 differential endogenous metabolites were identified as potential biomarkers related to the artesunate for treating malaria. These metabolites were mainly involved in the relevant pathways of biosynthesis of unsaturated fatty acids; aminoacyl-tRNA biosynthesis; valine, leucine, and isoleucine biosynthesis; and phenylalanine, tyrosine, and tryptophan biosynthesis. The results of the network pharmacology analysis showed 125 potential target genes related to the treatment of malaria with artesunate. The functional enrichment was mainly associated with lipid and atherosclerosis; pathways of prostate cancer and proteoglycans in cancer; and PI3K-Akt, apoptosis, NF-κB, Th17 cell, and AGE-RAGE signaling pathways. These findings were partly consistent with the findings of the metabolism. Our results further suggested that artesunate could correct the inflammatory response caused by malaria through Th17 cell and NF-κB pathways. Meanwhile, our work revealed that cholesterol needed by *Plasmodium berghei* came directly from serum. Cholesterol and palmitic acid may be essential in the growth and reproduction of *Plasmodium berghei*. In summary, artesunate may have an effect on anti-malarial properties through multiple targets.
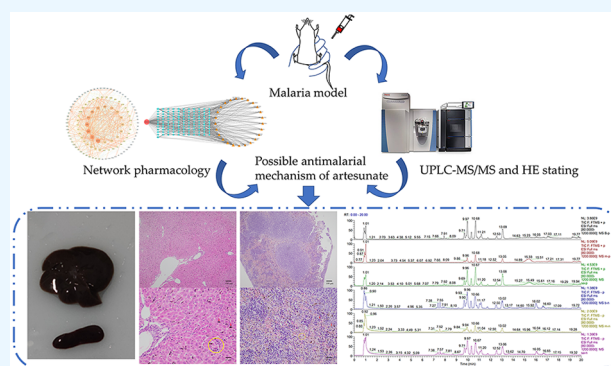
1. INTRODUCTION

The World Malaria Report 2021 issued by the World Health Organization (WHO) pointed out that the number of malaria cases increased to 2.41 million in 2020. Since 2000, the number of deaths caused by malaria has decreased year by year, although the number of deaths has increased in 2020.[1] Clearing malaria is still a great challenge. Malaria is an insect-borne infectious disease caused by *Anopheles* carrying *Plasmodium* (*P.*) biting or inputting the blood carrying *P.* There are two hosts during *P.* life: *Anopheles* and vertebrates. The stage of asexual reproduction in spinal animals is divided into two stages: intrahepatic phase and erythrocyte phase.[2,3] The metabolism of *P.* in the red phase is accelerated by the continuous consumption of hemoglobin to provide nutrients for their own division and proliferation. When *P.* develops into mature schizonts, a large number of schizonts are released from hepatocytes.[4] The proliferation of *P.* and the destruction of red blood cells caused a series of clinical symptoms, such as fever, anemia, and so forth.[5,6]

There are five main kinds of *P.* that infect humans: *Plasmodium falciparum*, *Plasmodium vivax*, *Plasmodium ovum*, *P. vivax*, and *Plasmodium knowlesi*.[7] There are two main species which infect rodents: *Plasmodium berghei* and *Plasmodium yoelii*.[4] The structure, physiology, and life cycle of *Plasmodium. berghei* ANKA (Pb) are similar to those of *P.* in primates.[8] Pb is often used to establish the model of mice malaria in the laboratory.
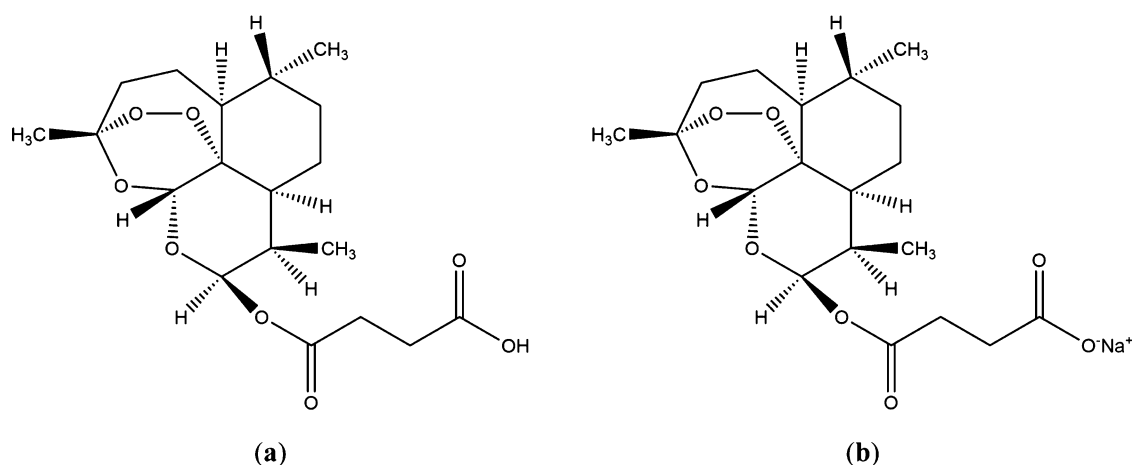
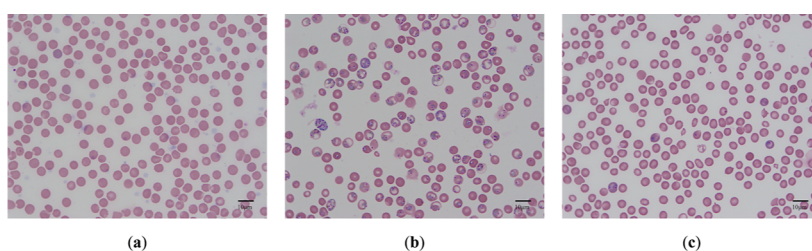**Figure 1.** Artesunate structure (a); SA structure (b).

Figure 2. Red blood cell Giemsa staining in the blank group (a), model group (b), and SA group (c).

Artemisinin and its derivatives are the most important class of anti-malarial drugs.[9] Artesunate is a semi-synthetic derivative of artemisinin (Figure 1a).[10] The mechanism of artemisinin and its derivatives, the most potent of the anti-malarial drugs, is not completely understood.[11] Most scholars believed that artesunate killed *P.* via the cleavage of their endoperoxide bridge by heme or iron.[12] There were some studies on specific targets of malaria. Wang et al., showed that heme was predominantly responsible for artemisinin activation. When artemisinin drugs were activated by heme, many proteins of *P.* were misfolded, resulting in irreversible protein damage.[13] In addition, artemisinin drugs could destroy multiple organelles such as mitochondria, endoplasmic reticulum, and digestive vacuoles of *P.*[14−16] However, the mechanism of artesunate in anti-malarial activity is not completely clear. Thus, artemisinin drugs may act on multiple organs and multiple targets to produce anti-malarial effects. However, the mechanism underlying the parasite's infection is largely unknown.

Our study used sodium artesunate (SA), which is the sodium salt form of artesunate (Figure 1b), and SA has better solubility than artesunate. Giemsa and hematoxylin and eosin (HE) staining were used to evaluate the efficacy of SA on malaria. Then, the network pharmacology was utilized to elucidate its molecular mechanisms in malaria and to construct the key "component–targets–pathways" network. In addition, the metabolomic was applied to study changes in endogenous substances induced by treatment with artesunate so that experimental evidence related to the metabolic mechanism of artesunate in treating Pb could be provided. This paper revealed the potential complex relationship between multiple metabolites and multiple targets by studying the effects of artesunate on endogenous metabolites and metabolic pathways in infected mice.

2. RESULTS

2.1. Giemsa Staining and Infection Rate. According to the results of Giemsa staining (Figure 2), it was observed that the model group contained late trophozoites and mass ring forms. In the model group, it was observed that the red blood cell structure was fragile, and the infection rate was $78.44 \pm 12.64\%$. The percentage parasitemia of the SA group was significantly lower than that of the model group, and the infection rate was $7.82 \pm 4.12\%$. The SA group contained a small amount of ring forms.

2.2. Histopathological. Three groups' mice showed a significant difference in color and shape of liver and spleen (Figure 3). The hepatomegaly and spleen of the model group for 5 days were enlarged, and the color of liver and spleen deepened. The organs were structurally fragile and easy to break during the experimental operation. However, the above symptoms were alleviated in the SA group.
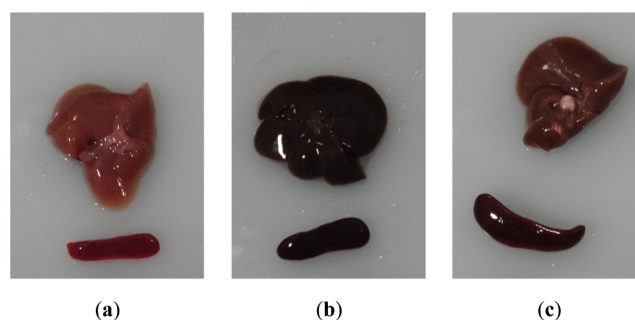

Figure 3. Liver and spleen morphology of Pb in the blank group (a), model group (b), and SA group (c).
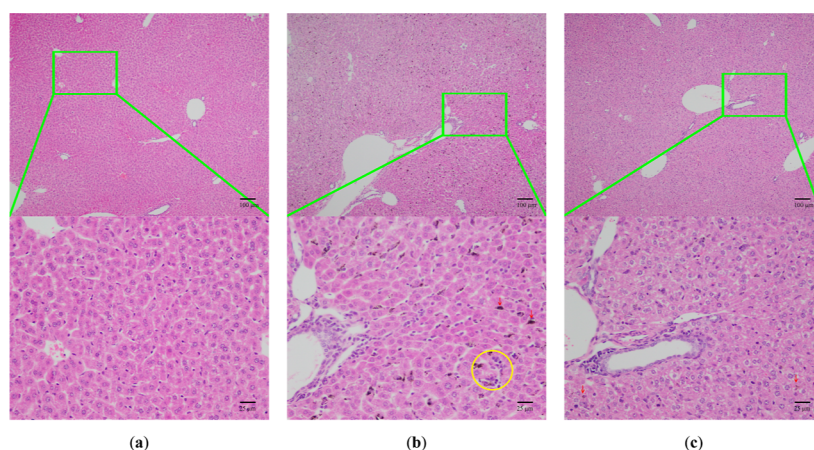
Figure 4. Morphology of the liver tissue of the blank group (a), model group (b), and SA group (c) infected by HE (100×, 400×). Red arrow: Pb remnant; yellow circle: inflammatory infiltration.
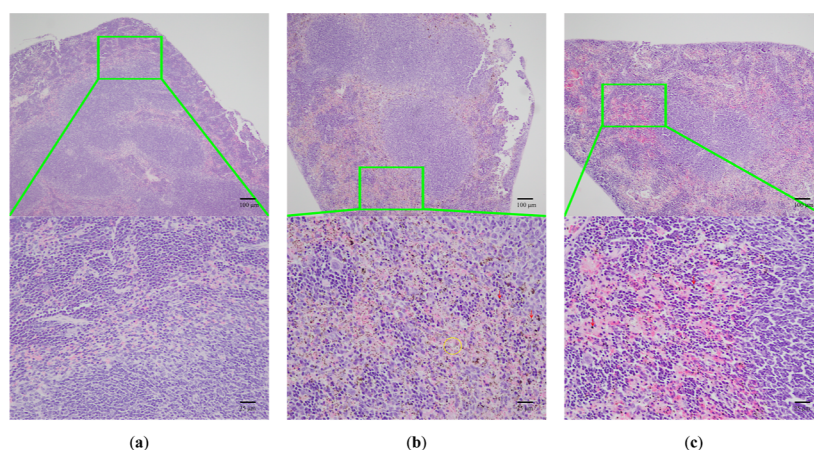

Figure 5. Morphology of the spleen tissue of the blank group (a), model group (b), and SA group (c) infected by HE (100×, 400×). Red arrow: Pb remnant; yellow circles: vacuolated lesions.

Inflammation and necrotic lesions (yellow circle) (Figure 4) were observed in the livers of model group mice. Furthermore, the liver cells with uneven sizes, extensive swelling, and loose tissues of hepatocytes were seen in the livers of the model group, and malarial pigment deposition was found in the livers of malarial mice (red arrow). However, all symptoms were relieved in the SA group.

The HE staining (Figure 5) of the spleen tissue showed a clear distinction between the red pulp and white pulp. Severe hyperemia and enlargement of the red pulp were observed in the model group. The structure of the white pulp was destroyed, and the clear marginal zones surrounding follicles became inapparent in spleens of infected mice. Furthermore, extensive vacuolation in the red pulp was acquired in spleens of model group mice (yellow circle). The malarial pigment deposition was observed in the livers of model mice on day 5 after infection (red arrow). However, all symptoms were relieved in the SA group.

2.3. Metabolomics. *2.3.1. Multivariable Data Analysis.* Figure 6 shows the typical ultra-high-performance liquid chromatography tandem mass spectrometry (UHPLC-MS/MS) total ion current chromatogram of serum samples. Meanwhile, quality control (QC) samples could cluster together, indicating that the instrument was stable (Figure 7). PCA and PLS-DA (ESI$^+$: R_2 = 0.0, 0.995, Q_2 = 0.0,

−0.0985; ESI$^-$: R_2 = 0.0, 0.677, Q_2 = −0.503) showed that the blank group, model group, and SA group were separated from each other and reflected the regulatory effect of SA on metabolites.

2.3.2. Identification of Differential Biomarkers. VIP was used to identify characteristic metabolites in the three groups, namely, ions with VIPs > 1.0, P < 0.05, and FC > 1.5 or FC < 0.67, which were considered potential biomarkers. In the positive ion mode, eight differential endogenous metabolites were putatively identified among the blank group, model group, and SA group. Similarly, 11 metabolites were identified in the negative ion mode as differential metabolites among three groups. Detailed information regarding each differential metabolite is provided in Table 1.

In negative ion and positive ion modes, contrary to the blank group, the integral levels of L-histidine, D-leucine, L-leucine, and L-phenylalanine were increased in the model group. Notably, the levels of these metabolites were decreased in the SA group. In contrast to the blank group, expressions of 11,12-epoxyeicosatrienoic acid, palmitic acid, stearic acid, linoleic acid, and tetradecanedioic acid were downregulated in the model group. After treatment with SA, the levels of these metabolites increased. Similarly, in the positive ion mode, the levels of L-isoleucine, D-ornithine, D-proline, proline betaine, and cytidine were increased in the model group compared with
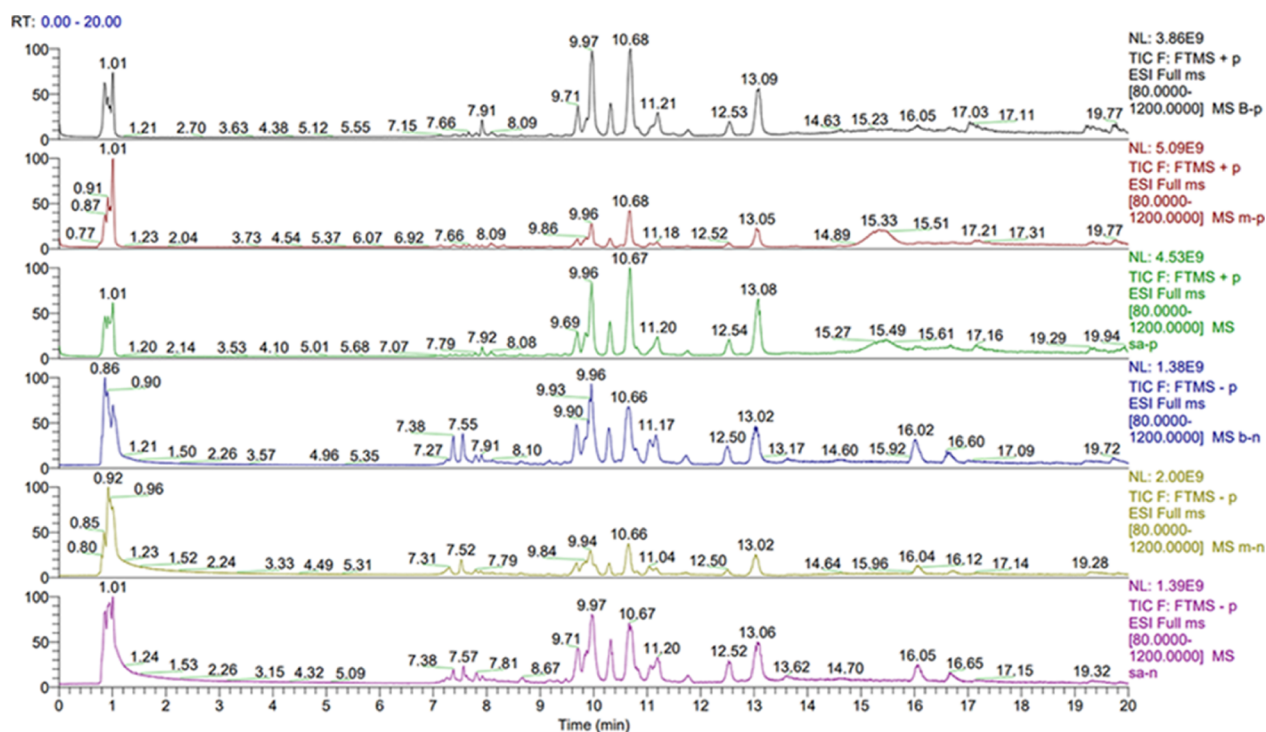
Figure 6. Typical UHPLC-MS/MS total ion currents of serum samples. Black and blue indicate the total ion flow diagrams of the blank group; red and yellow indicate the total ion flow diagrams of the model group; green and purple indicate the total ion flow diagrams of the SA group.

(a) **(b)**
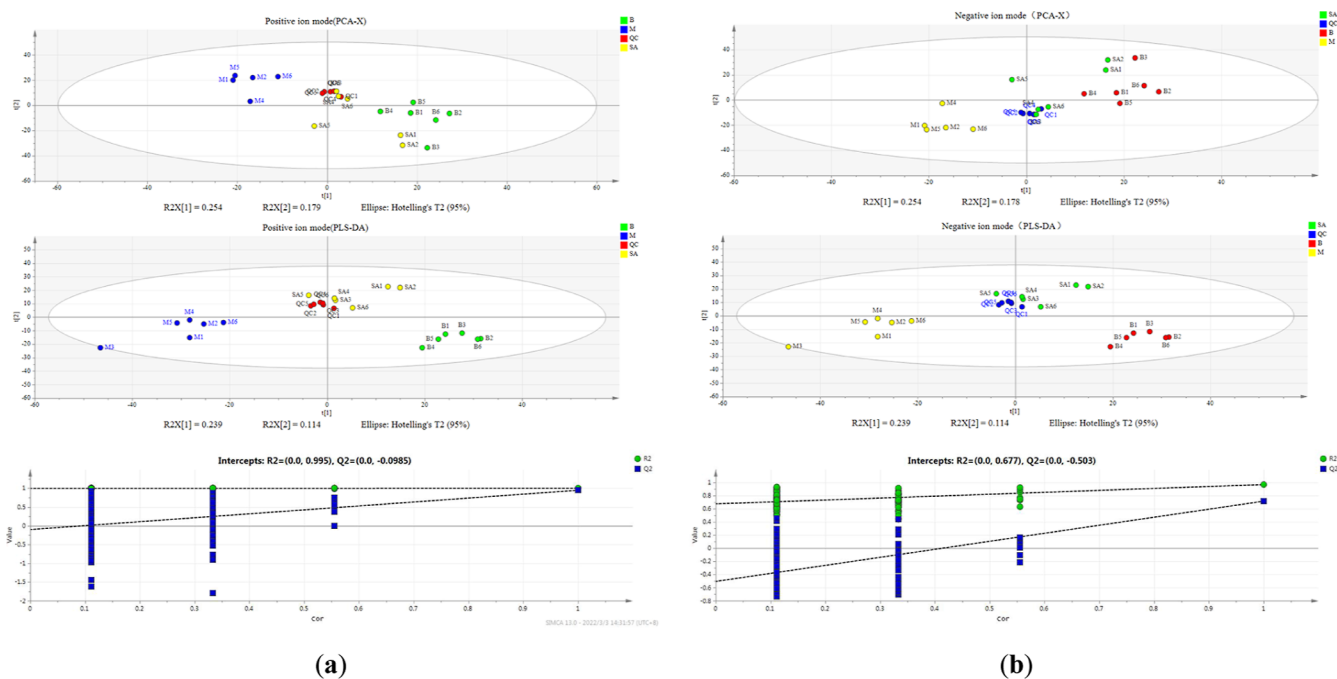
Figure 7. Results of multivariate statistical analysis. The positive ion mode (a); the negative ion mode (b).

the blank group. In contrast, the integral levels of eicosapentaenoic acid and 17-HDoHE were decreased in the model group compared with the blank group. Interestingly, intervention with SA reversed these alterations induced by the model group.

The heat maps average normalized amount of differentially expressed metabolites in the three groups and showed that metabolite expression varied significantly between different groups (Figure 8).

2.3.3. Metabolic Pathways Analysis. A total of 18 differential endogenous metabolites were found among the three groups. They were associated mainly with fatty acids, amino acid, and phosphatide. Metabolic pathway analysis was carried out by importing these differential endogenous metabolites into MetaboAnalyst 5.0 to further explore the possible mechanisms through which there is SA treatment of malaria. We obtained 25 metabolic pathways through this analytical method (Figure 9) by setting the screening threshold

Table 1. Differential Metabolites Characterized in the Serum Profile and Their Change Trend after SA Treatment

no.	RT	metabolite identification	HMDB	formula	m/z	ion from	P (SA[b]/M[c])	SA/M	P (M/B[d])	M/B
1	11.060	11,12-epoxyeicosatrienoic acid	HMDB0004673	$C_{20}H_{32}O_3$	319.2279	$[M-H]^-$	1.40×10^{-1}		2.04×10^{-2}	↓
2	0.849	L-histidine	HMDB0000177	$C_6H_9N_3O_2$	154.2000	$[M-H]^-$	1.84×10^{-10}	↓	3.25×10^{-12}	↑
3	10.299	palmitic acid	HMDB0000220	$C_{16}H_{32}O_2$	256.2350	$[M-H]^-$	3.61×10^{-2}	↑[a]	4.88×10^{-2}	↓
4	12.430	stearic acid	HMDB0000827	$C_{18}H_{36}O_2$	283.2647	$[M-H]^-$	3.98×10^{-2}	↑	3.60×10^{-2}	↓
5	17.930	linoleic acid	HMDB0000673	$C_{18}H_{32}O_2$	279.4000	$[M-H]^-$	4.39×10^{-2}	↑	4.66×10^{-2}	↓
6	8.660	tetradecanedioic acid	HMDB0000872	$C_{14}H_{26}O_4$	257.1758	$[M-H]^-$	5.90×10^{-3}	↑	3.26×10^{-2}	↓
7	1.110	D-leucine	HMDB0013773	$C_6H_{13}NO_2$	130.0874	$[M-H]^-$	3.22×10^{-2}	↓	1.59×10^{-2}	↑
8	1.110	L-leucine	HMDB0000687	$C_6H_{13}NO_2$	130.0874	$[M-H]^-$	3.22×10^{-2}	↓	1.59×10^{-2}	↑
9	10.780	oleic acid	HMDB0000207	$C_{18}H_{34}O_2$	282.2509	$[M-H]^-$	8.24×10^{-4}	↑	2.70×10^{-3}	
10	1.040	L-phenylalanine	HMDB0000159	$C_9H_{11}NO_2$	163.9000	$[M-H]^-$	1.43×10^{-2}	↓	1.28×10^{-3}	↑
11	0.890	L-isoleucine	HMDB0000172	$C_6H_{13}NO_2$	131.9010	$[M+H]^+$	2.99×10^{-2}	↓	1.24×10^{-2}	↑
12	0.903	L-ornithine	HMDB0003374	$C_5H_{12}N_2O_2$	132.9620	$[M+H]^+$	1.06×10^{-4}	↓	6.79×10^{-4}	↑
13	1.000	D-proline	HMDB0003411	$C_5H_9NO_2$	114.0560	$[M+H]^+$	1.41×10^{-5}	↓	5.87×10^{-4}	↑
14	0.910	proline betaine	HMDB0004827	$C_7H_{13}NO_2$	144.1019	$[M+H]^+$	2.60×10^{-5}	↓	9.47×10^{-3}	↑
15	9.770	eicosapentaenoic acid	HMDB0001999	$C_{20}H_{30}O_2$	303.2319	$[M+H]^+$	1.96×10^{-2}	↑	8.57×10^{-3}	↓
16	7.770	cytidine	HMDB0000089	$C_9H_{13}N_3O_5$	243.9400	$[M+H]^+$	1.23×10^{-2}	↓	2.32×10^{-5}	↑
17	9.110	choline	HMDB0000097	$C_5H_{13}NO$	105.5000	$[M+H]^+$	2.81×10^{-2}	↑	6.68×10^{-2}	↓
18	7.780	17-HDoHE	HMDB0010213	$C_{23}H_{32}O_3$	357.2424	$[M+H]^+$	1.13×10^{-1}		2.43×10^{-2}	↓

[a]Arrow ↑ means a relative increase in signal; arrow ↓ means a relative decrease in signal. [b]SA means sodium artesunate. [c]M means the model group. [d]B means the blank group.
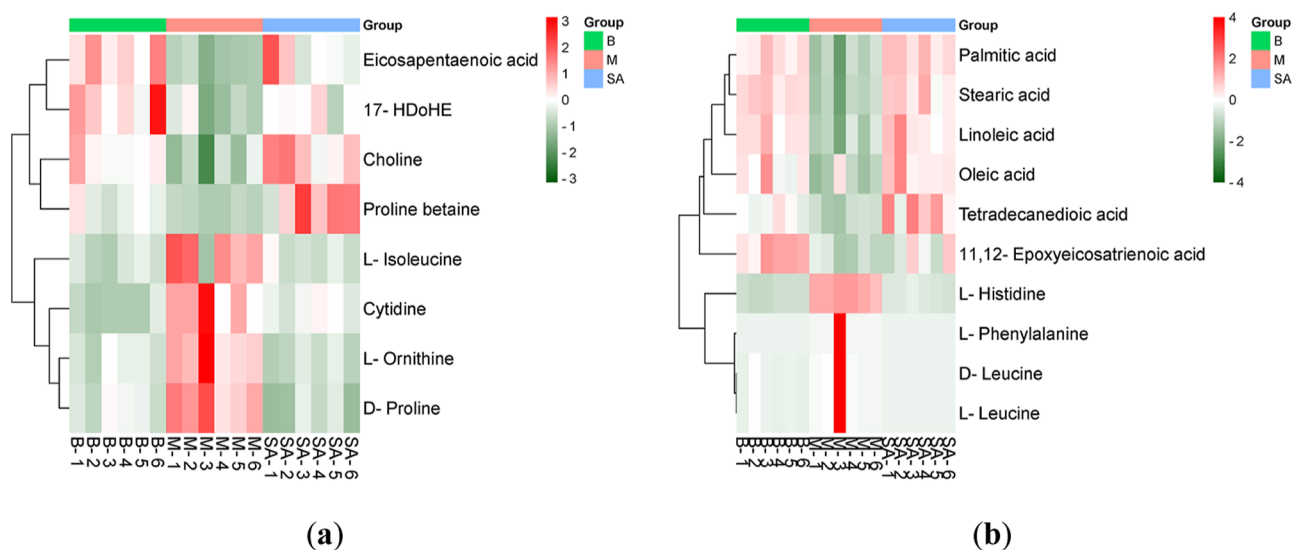
Figure 8. Results of multivariate statistical analysis. The positive ion mode (a); the negative ion mode (b).

as raw $P < 0.05$ and pathway impact value > 0.1.[17] We obtained the biosynthesis of unsaturated fatty acids; amino-acyl-tRNA biosynthesis; valine, leucine, and isoleucine biosynthesis; and phenylalanine, tyrosine, and tryptophan biosynthesis as key metabolic pathways.

2.4. Targets Prediction of Artesunate on Malaria. We retrieved the targets of artesunate from databases and related publications. Moreover, 317 predicted targets of artesunate were identified based on the obtained compounds. Matching them with the malaria-related targets acquired through OMIM and GeneCard, we finally identified 122 potential targets of artesunate related to malaria treatment. We acquired 125 pathways including lipid and atherosclerosis; pathways in cancer, prostate cancer, and proteoglycans in cancer; PI3K-Akt signaling pathway; apoptosis; Hepatitis B, IL-17 signaling pathway, AGE-RAGE signaling pathway in diabetic complications and so on (Figure 10a).

After extracting the relationship information for the 122 potential target genes of artesunate, a protein−protein interaction network was constructed, as shown in Figure 10b. There were some central nodes in the network, such as heat shock protein HSP 90-alpha, protooncogene tyrosine-protein kinase Src, caspase-3, epidermal growth factor receptor, and signal transducer and activator of transcription 3. These results suggested that amino acid metabolism and inflammatory genes may be the key target genes for artesunate to treatment malaria (Figure 10b).

Gene Ontology (GO) and Kyoto Encyclopedia of Genes and Genomes (KEGG) pathway enrichment analyses were undertaken to explore the potential functions of the 122 potential target genes of artesunate acting on malaria. The top 10 enriched GO terms ranked by P-value in biological processes, cell components, and molecular functions are presented in Figure 11a. The top three terms in GO biological processes were regulation of programmed cell death (GO:0043067), regulation of the apoptotic process (GO:0042981), and the apoptotic process (GO:0006915). In terms of GO cell components, they were mainly enriched in
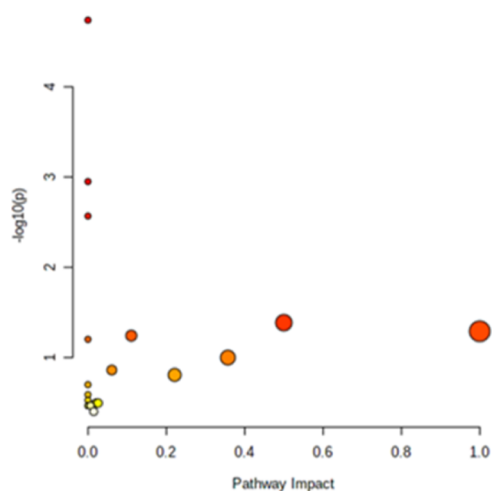
Figure 9. Pathways analyses of differential metabolites in the serum sample.

ficolin-1-rich granules (GO:0101002), ficolin-1-rich granule lumen (GO:1904813), and the cytoplasmic part (GO:0044444). Regarding GO molecular functions, the terms were catalytic activity (GO:0003824), enzyme binding (GO:0019899), and peptidase activity, acting on L-amino acid peptides (GO:0070011). GO and KEGG pathway enrichment analyses were accomplished for further investigation of the potential functions of the detected targets ($P < 0.05$). According to the KEGG enrichment analysis, lipid and atherosclerosis (hsa05417) and pathways in cancer (hsa05200) were significantly enriched, as shown in Table 2 and Figure 11b.

We focused on the correlation of metabolites and possible targets to integrate the results of metabolomics and network pharmacology and comprehensively explored the underlying mechanisms. We specifically referred to the relationship between metabolites of crucial pathways and their related proteins. Ultimately, a network containing relationships between metabolites, metabolic pathways, and enzymes was established (Figure 12).

3. DISCUSSION

Malaria is a disease caused by *P.* parasites transmitted through the bites by the infected *Anopheles*. After 1 to 3 h, the sporozoites leave the skin and are brought to the liver cells.[18] The Trap like protein was necessary to *P.* to enter liver cells.[19] The first replication of *P.* needed some specific proteins, such as sporozoite microneme protein essential for cell traversal, perforin-like protein 1, phosphlipase A2, and so on.[19−21] In summary, erythrocyte invasion by *P.* is a tight process involving a series of receptor−ligand interactions.

Studies suggested that the possible endogenous metabolite biomarkers in the development and progression of malaria include histidine, linoleic acid, tetradecanedioic acid, leucine, oleic acid, phenylalanine, isoleucine, ornithine, proline, proline betaine, eicosapentaenoic acid, cytidine, choline, and so on. From Table 1, we could know that the differential metabolites in serum were mainly concentrated in the process of amino acid and lipid metabolism. Moreover, four metabolic pathways were predicted to be associated with SA treatment by malaria. The results of the network pharmacology analysis showed 122 potential target genes and 125 pathways related to the treatment of malaria with artesunate. The results of network pharmacology were partly consistent with the experimental results. The disease mainly affects amino acid and fatty acid metabolism in mice.

Proliferation of *P.* in host cells requires a large amount of protein synthesis, which might be the reason for the disorder of amino acid metabolism caused by *P.* Wang et al., who identified 124 target proteins of artemisinin by chemical proteomics.[13] Through the experimental results (Figure 12), we found that the synthetic pathways of L-histidine, L-phenylalanine, L-isoleucine, and L-ornithine were blocked under disease conditions. They could synthesize anserine, 5-formimidoyltetrahydrofolic acid, 4-fumarylacetoacetate, 5,6,7,8-tetrahydrobiopterin, and S-adenosylmethioninaminium. These compounds have the functions of antioxidant, anti-anemia, anti-nervous degeneration, anti-metabolism disorder, and maintenance of DNA methylation.[22−26] These synthetic products might play a vital role in the anti-malarial properties of SA.

HE staining showed that SA could inhibit liver and spleen inflammation caused by Pb. SA could be rapidly hydrolyzed to
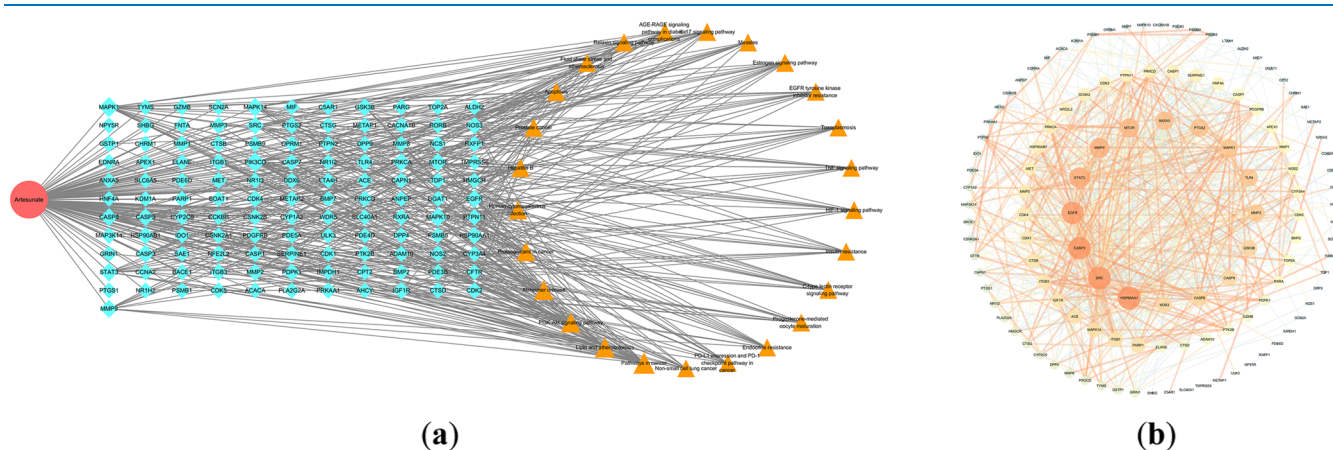

(a)

(b)

Figure 10. Drug−targets-pathways; the red, orange, and blue nodes represent the active drug, target genes, and pathways, respectively (a). Protein−protein interaction network of artesunate acting on malaria, the ranking of artesunate target genes' importance for treating malaria. The size and color of nodes were proportional to their degree value (b).
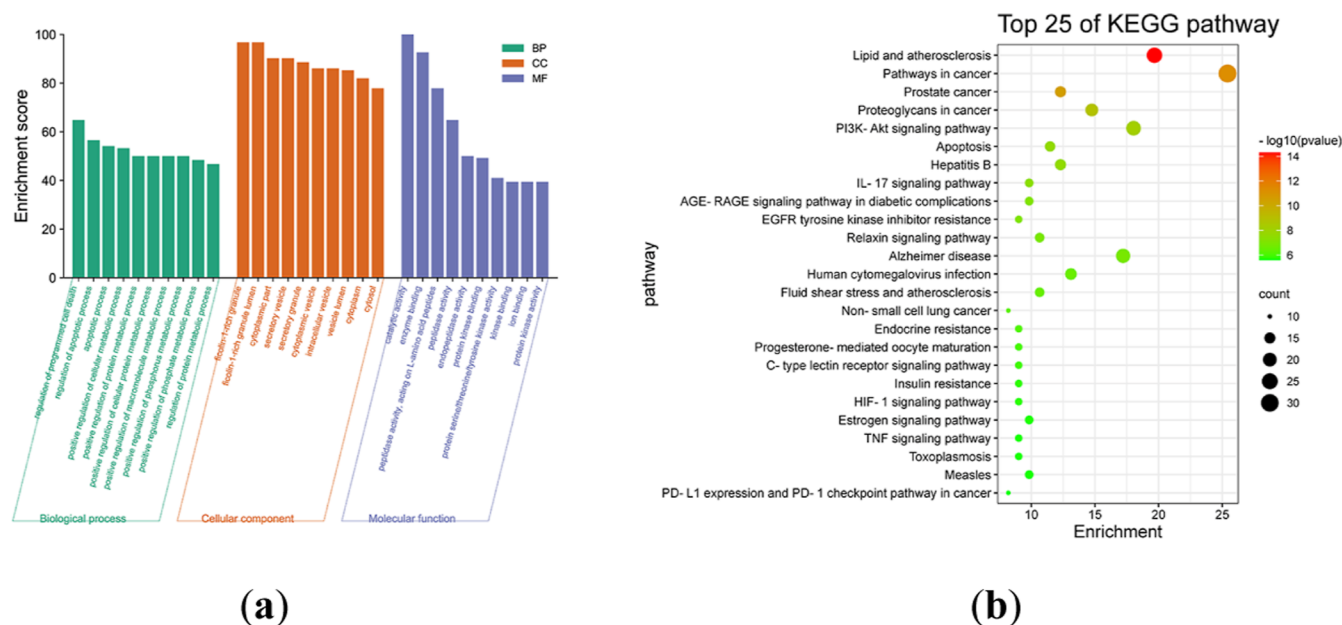
(a)

(b)

Figure 11. GO functional analysis (a). Bubble diagram of the KEGG pathway: the abscissa corresponds to the ratio of the pathway, the ordinate represents the KEGG term, the color of the sports corresponds to the −lg P, and the size of the dots corresponds to the number of genes annotated (b).

dihydroartemisinin in vivo.[27] SA regulated NF-κB, ERK, AMPK/SIRT1, and ROS-JNK1/2 inflammatory pathways.[28−31] Besides, the network pharmacology result showed that the therapeutic effect of artesunate on malaria was related to Th17 cell differentiation. Th17 cells played an important role in the autoimmune diseases and tissue inflammation. Th17 cells could increase the secretion of proinflammatory factors such as TNF, IL-1β, IL-6, and IL-8 by secreting inflammatory mediators IL-17. These inflammatory factors mediated the local infiltration of inflammatory cells and induce tissues.[32] Serum metabolomics results showed that L-phenylalanine was significantly increased in the model group, which may be a result of Pb inhibiting the synthesis of 3-(indol-3-yl) pyruvic acid. Studies demonstrated that 3-(indol-3-yl) pyruvic acid was an aromatic receptor activator.[33] Previously, scholars found that aromatic hydrocarbon receptor-mediated inflammation control was an important target of immunoregulation. Ligand activated aromatic hydrocarbon receptors could inhibit the differentiation, maturation, and function of dendritic cells. At the same time, the activated aromatic hydrocarbon receptor could reduce the expression of cytokines closely related to Th17 cell differentiation, such as IL-1β, IL-6, IL-23, and TNF-α. In this way, Th17 cell differentiation was inhibited.[34] When Pb infected mice, these acquired an increased accumulation of IL-17+ cells in the spleen tissue.[35] Artesunate attenuated inflammation by downregulating Th17 cell responses in mice.[10] This pathway may be a key for the artesunate to reduce inflammation and produce the anti-malarial effect.

Merozoites were released into the bloodstream from erythrocytes infected by Pb, and they enabled attachment to nearby erythrocytes.[5,36] Pb could not only change the structure membrane but also change the function of red blood cells, and these changes made red blood cells more suitable for the growth and reproduction of Pb.[37−39] Pb increased phosphatidylcholine content in the host cell membrane.[40] Phosphatidylcholine was the main membrane phospholipids of *P. parasites* and could be generated by the Kennedy CDP-choline

pathway; the Kennedy pathways initiate from choline.[41] However, the exact source of choline was not clear, and most scholars believed that it came directly from the serum.[42] Network pharmacology results showed that artesunate had anti-malarial effects by affecting choline metabolism. Our experimental results reinforced the hypothesis that choline required for Pb came from serum. The content of choline in the host serum of the model group decreased significantly, so we speculated that the phenomenon may be related to the synthesis of phosphatidylcholine by Pb using the choline of the host.[40] The content of phosphatidylcholine in infected red blood cells will increase.[43] At the same time, the excessive synthesis of phosphatidylcholine reduced the content of choline in serum, while a lack of choline affected the synthesis of acetylcholine.[44] Acetylcholine was released at nerve terminals, and the neurotransmitters could activate immune cells located in close proximity to the nerve terminals such as macrophages.[45] Expression of receptors for neurotransmitters was found in the α7 subunit of the nicotinic acetylcholine receptor on macrophages. Activation of the receptor inhibited the release of proinflammatory factors such as tumor necrosis factor-α.[46] In summary, the cholinergic anti-inflammatory pathway produced anti-inflammatory effects by regulating the NF-κB pathway.[47] Pb could activate the host NF-κB pathway.[48] Inflammatory mice treated with SA showed downregulating NF-κB phosphorylation.[49] These results are consistent with our experimental results. Our experimental results showed that SA reduced the release of inflammatory factors through downregulating the NF-κB pathway to reduce the release of inflammatory factors and then to improve the inflammation of the host liver and spleen.

In contrast to the blank group, palmitic acid was downregulated in the model group. After treatment with SA, the levels of palmitic acid increased. Previous studies have shown an increased content of palmitic acid in infected erythrocyte plasma infected with Pb.[50] We speculate that palmitic acid plays an important role in the growth and

Table 2. Main KEGG Pathways Significantly Relating to Major Hubs

term	pathway	count	pop hits	P-value	term	pathway	count	pop hits	P-value
hsa05417	lipid and atherosclerosis	24	215	4.88×10^{-15}	hsa04020	calcium signaling pathway	12	240	3.49×10^{-4}
hsa05200	pathways in cancer	31	531	5.72×10^{-12}	hsa04520	adherens junction	7	71	3.54×10^{-4}
hsa05215	prostate cancer	15	97	2.82×10^{-11}	hsa05169	Epstein−Barr virus infection	11	202	3.56×10^{-4}
hsa05205	proteoglycans in cancer	18	205	1.44×10^{-9}	hsa05218	melanoma	7	72	3.82×10^{-4}
hsa04151	PI3K-Akt signaling pathway	22	354	6.42×10^{-9}	hsa04115	p53 signaling pathway	7	73	4.12×10^{-4}
hsa04210	apoptosis	14	136	2.64×10^{-8}	hsa05165	human papillomavirus infection	14	331	4.50×10^{-4}
hsa05161	hepatitis B	15	162	2.71×10^{-8}	hsa04660	T-cell receptor signaling pathway	8	104	4.64×10^{-4}
hsa04657	IL-17 signaling pathway	12	94	4.06×10^{-8}	hsa04910	insulin signaling pathway	9	137	4.77×10^{-4}
hsa04933	AGE-RAGE signaling pathway in diabetic complications	12	100	7.78×10^{-8}	hsa04659	Th17 cell differentiation	8	108	5.83×10^{-4}
hsa01521	EGFR tyrosine kinase inhibitor resistance	11	79	8.12×10^{-8}	hsa05152	tuberculosis	10	180	6.59×10^{-4}
hsa04926	relaxin signaling pathway	13	129	1.27×10^{-7}	hsa04621	NOD-like receptor signaling pathway	10	184	7.72×10^{-4}
hsa05010	Alzheimer disease	21	384	1.36×10^{-7}	hsa04670	leukocyte transendothelial migration	8	114	8.06×10^{-4}
hsa05163	human cytomegalovirus infection	16	225	2.66×10^{-7}	hsa04215	apoptosis—multiple species	5	32	8.19×10^{-4}
hsa05418	fluid shear stress and atherosclerosis	13	139	2.90×10^{-7}	hsa05134	legionellosis	6	57	9.44×10^{-4}
hsa05223	non-small cell lung cancer	10	72	4.17×10^{-7}	hsa05213	endometrial cancer	6	58	1.02×10^{-3}
hsa01522	endocrine resistance	11	98	6.39×10^{-7}	hsa04071	sphingolipid signaling pathway	8	119	1.04×10^{-3}
hsa04914	progesterone-mediated oocyte maturation	11	102	9.29×10^{-7}	hsa04935	growth hormone synthesis, secretion, and action	8	119	1.04×10^{-3}
hsa04625	C-type lectin receptor signaling pathway	11	104	1.11×10^{-6}	hsa04722	neurotrophin signaling pathway	8	119	1.04×10^{-3}
hsa04931	insulin resistance	11	108	1.58×10^{-6}	hsa04014	Ras signaling pathway	11	232	1.05×10^{-3}
hsa04066	HIF-1 signaling pathway	11	109	1.72×10^{-6}	hsa04932	non-alcoholic fatty liver disease	9	155	1.08×10^{-3}
hsa04915	estrogen signaling pathway	12	138	2.07×10^{-6}	hsa04217	necroptosis	9	159	1.27×10^{-3}
hsa04668	TNF signaling pathway	11	112	2.21×10^{-6}	hsa04611	platelet activation	8	124	1.32×10^{-3}
hsa05145	toxoplasmosis	11	112	2.21×10^{-6}	hsa05203	viral carcinogenesis	10	204	1.60×10^{-3}
hsa05162	measles	12	139	2.22×10^{-6}	hsa05132	Salmonella infection	11	249	1.79×10^{-3}
hsa05235	PD-L1 expression and PD-1 checkpoint pathway in cancer	10	89	2.58×10^{-6}	hsa05164	Influenza A	9	171	2.02×10^{-3}
hsa05415	diabetic cardiomyopathy	14	203	2.79×10^{-6}	hsa04664	Fc epsilon RI signaling pathway	6	68	2.09×10^{-3}
hsa05120	epithelial cell signaling in *Helicobacter pylori* infection	9	70	3.78×10^{-6}	hsa04920	adipocytokine signaling pathway	6	69	2.23×10^{-3}
hsa05022	pathways of neurodegeneration—multiple diseases	21	476	4.04×10^{-6}	hsa05230	central carbon metabolism in cancer	6	70	2.38×10^{-3}
hsa05207	chemical carcinogenesis—receptor activation	14	212	4.52×10^{-6}	hsa05206	MicroRNAs in cancer	12	310	2.81×10^{-3}
hsa05133	pertussis	9	76	7.06×10^{-6}	hsa05140	leishmaniasis	6	77	3.61×10^{-3}
hsa05167	Kaposi sarcoma-associated herpesvirus infection	13	194	9.89×10^{-6}	hsa04072	phospholipase D signaling pathway	8	148	3.62×10^{-3}
hsa04370	VEGF signaling pathway	8	59	1.22×10^{-5}	hsa05226	gastric cancer	8	149	3.75×10^{-3}
hsa04510	focal adhesion	13	201	1.42×10^{-5}	hsa04726	serotonergic synapse	7	115	4.33×10^{-3}
hsa05219	bladder cancer	7	41	1.54×10^{-5}	hsa04150	mTOR signaling pathway	8	156	4.83×10^{-3}
hsa04936	alcoholic liver disease	11	142	1.86×10^{-5}	hsa04010	MAPK signaling pathway	11	294	5.87×10^{-3}
hsa05222	small cell lung cancer	9	92	2.92×10^{-5}	hsa04540	gap junction	6	88	6.37×10^{-3}
hsa04152	AMPK signaling pathway	10	120	3.01×10^{-5}	hsa00591	linoleic acid metabolism	4	29	6.62×10^{-3}
hsa04912	GnRH signaling pathway	9	93	3.16×10^{-5}	hsa04650	natural killer cell-mediated cytotoxicity	7	126	6.74×10^{-3}
hsa04919	thyroid hormone signaling pathway	10	121	3.21×10^{-5}	hsa00590	arachidonic acid metabolism	5	61	8.83×10^{-3}
hsa05208	chemical carcinogenesis—reactive oxygen species	13	223	3.99×10^{-5}	hsa04024	cAMP signaling pathway	9	221	9.42×10^{-3}
hsa04613	neutrophil extracellular trap formation	12	190	4.38×10^{-5}	hsa04750	inflammatory mediator regulation of TRP channels	6	98	9.95×10^{-3}
hsa05160	hepatitis C	11	157	4.42×10^{-5}	hsa04371	apelin signaling pathway	7	139	1.07×10^{-2}
hsa01524	platinum drug resistance	8	73	5.00×10^{-5}	hsa05146	amebiasis	6	102	1.17×10^{-2}
hsa05171	coronavirus disease—COVID-19	13	232	5.87×10^{-5}	hsa05017	spinocerebellar ataxia	7	143	1.22×10^{-2}
hsa05214	glioma	8	75	5.96×10^{-5}	hsa05221	acute myeloid leukemia	5	67	1.22×10^{-2}
hsa04068	FoxO signaling pathway	10	131	6.02×10^{-5}	hsa04064	NF-kappa B signaling pathway	6	104	1.26×10^{-2}

Table 2. continued

| term	pathway	count	pop hits	P-value	term	pathway	count	pop hits	P-value
hsa05130	pathogenic *Escherichia coli* infection	12	197	6.10×10^{-5}	hsa04620	toll-like receptor signaling pathway	6	104	1.26×10^{-2}
hsa05142	chagas disease	9	102	6.16×10^{-5}	hsa04960	aldosterone-regulated sodium reabsorption	4	37	1.30×10^{-2}
hsa05212	pancreatic cancer	8	76	6.49×10^{-5}	hsa05204	chemical carcinogenesis—DNA adducts	5	69	1.35×10^{-2}
hsa05020	prion disease	14	273	6.68×10^{-5}	hsa05224	breast cancer	7	147	1.38×10^{-2}
hsa05225	hepatocellular carcinoma	11	168	7.85×10^{-5}	hsa05202	transcriptional misregulation in cancer	8	193	1.47×10^{-2}
hsa05135	Yersinia infection	10	137	8.53×10^{-5}	hsa04921	oxytocin signaling pathway	7	154	1.71×10^{-2}
hsa04140	autophagy—animal	10	141	1.07×10^{-4}	hsa04630	JAK-STAT signaling pathway	7	162	2.13×10^{-2}
hsa05131	Shigellosis	13	247	1.07×10^{-4}	hsa04810	regulation of actin cytoskeleton	8	218	2.67×10^{-2}
hsa04015	Rap1 signaling pathway	12	210	1.08×10^{-4}	hsa04380	osteoclast differentiation	6	128	2.83×10^{-2}
hsa05170	human immunodeficiency virus 1 infection	12	212	1.18×10^{-4}	hsa05032	morphine addiction	5	91	3.34×10^{-2}
hsa04012	ErbB signaling pathway	8	85	1.33×10^{-4}	hsa04614	renin—angiotensin system	3	23	3.74×10^{-2}
hsa05210	colorectal cancer	8	86	1.43×10^{-4}	hsa04923	regulation of lipolysis in adipocytes	4	56	3.88×10^{-2}
hsa04360	axon guidance	11	182	1.53×10^{-4}	hsa04550	signaling pathways regulating pluripotency of stem cells	6	143	4.26×10^{-2}
hsa04218	cellular senescence	10	156	2.30×10^{-4}	hsa04062	chemokine signaling pathway	7	192	4.37×10^{-2}
hsa05231	choline metabolism in cancer	8	98	3.23×10^{-4}	hsa04723	retrograde endocannabinoid signaling	6	148	4.82×10^{-2}
hsa04917	prolactin signaling pathway	7	70	3.28×10^{-4}	hsa04213	longevity regulating pathway—multiple species	4	62	5.00×10^{-2}
hsa04930	type II diabetes mellitus	6	46	3.47×10^{-4}					
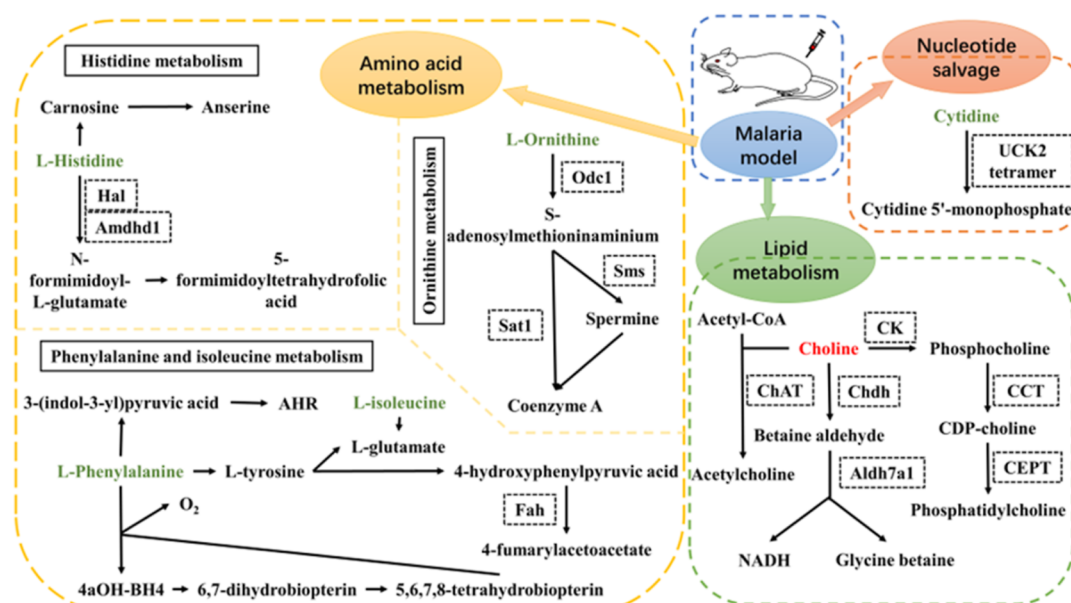
Figure 12. Proposed metabolic pathways for explanation relationship between SA and malaria treatment in serum. Red represents the upregulation of metabolites. Green represents the downregulation of metabolites.

reproduction of Pb. However, this speculation still needs further verification.

Combining previous research and our studies, we hypothesized that artesunate may act on malaria through different biological pathways. Three limitations should be considered in the interpretation of our findings. First, further pharmacological experiments are necessary to validate the accurate mechanisms of artesunate predicted by the network pharmacology analysis. Second, comprehensive metabolic changes in other structures (e.g., spinal fluid, liver) should be determined to more accurately reflect the mechanism through

which artesunate acts on malaria. Third, enhanced metabolomics technologies, such as targeted metabolomics, are required to detect metabolite biomarkers purposefully.

4. MATERIALS AND METHODS

4.1. Materials and Reagents. *Plasmodium berghei* ANKA strain artesunate (100 g, batch number: X03511Y123220) was purchased from source leaf organisms (Shanghai, China). UHPLC grade methanol was provided by Merck (Canada). Formic acid and acetonitrile were supplied by Thermo Fisher

Scientific (Fair Lawn, NJ, USA). Water was obtained from Watsons (Guangdong, China).

Vanquish UHPLC (Thermo Scientific, Germany) equipped with a vanquish autosampler, a vanquish pump, and a vanquish column compartment; a Q-Exactive Plus Orbitrap MS (Thermo Scientific, Germany), and an X-30R all-purpose high-speed freeze centrifuge (Berle X-mark, USA) were used.

4.2. Experimental Design. The study protocol was approved by the Animal Experimental Ethics Committee of Shandong Academy of Traditional Chinese Medicine (protocol code SDZYY20200415002 and 15 Apr 2020 of approval).

SPF female KM mice (18 ± 2 g) were obtained from Beijing Vital River Laboratory Animal Technology Co., Ltd., license number: SCXK (Beijing) 2016-0011. All mice were raised in the Shandong Institute of Traditional Chinese Medicine animal room and were housed under standard conditions (55 ± 5% relative humidity, 12 h light−dark cycle, 22 ± 2 °C) and had free access to standard mice chow and water. A total of 18 mice were divided equally and randomly into a blank group, model group, and SA group. All animals that died because of Pb were disposed by incineration.

After 7 days of adaptive feeding, each model group and SA group mice were infected with 2×10^7 Pb infected erythrocytes, whereas the blank group received an equal amount of normal saline. We injected the mice with drugs 2 h after the Pb infection. Mice in the SA group were received i.p. of 1 mg artesunate/20 g mice bodyweight, while the blank group and model group received an equal amount of normal saline. All mice were continuously i.p. administrated for 4 days.

4.3. Giemsa Staining. The 5 days post-infection levels of parasitemia were determined by microscopic examination of Giemsa-stained thin blood smears of peripheral tail blood of each mouse.[51,52] All the smears were air dried with high purity nitrogen and fixed in methanol. Finally, samples were stained for 20 min. The formula % parasitemia = [(total number of infected RBC counted/total number of RBC counted) × 100] was used.

4.4. HE Staining. Mice livers and spleens were fixed in 4% paraformaldehyde at room temperature for ≥24 h. After paraffin embedding and slicing, HE staining was performed to determine changes of hepatic and splenic architectures.[53]

4.5. UHPLC-MS/MS-Based Serum Metabolomics. *4.5.1. Collection and Preparation of Samples.* After Giemsa staining, mice were followed by a cardiac puncture to collect blood in a centrifuge tube. Samples were stored at room temperature for more than half an hour. Subsequently, the serum was separated by centrifugation (3000 rpm, 10 min, 4 °C) and stored at −200 °C until use. The process of sample preparation for UHPLC-MS/MS was very specific. First, methanol (300 μL) was added to a serum sample (100 μL), after which it was vortex-mixed for 1 min; then the sample was separated by centrifugation (12,000 rpm, 10 min, 4 °C). Subsequently, the supernatant was subjected to nitrogen drying and redissolved in methanol (100 μL). The experimenter took 20 μL of each sample and mixed it as the QC sample of UHPLC-MS/MS.

4.5.2. Acquisition of UHPLC-MS/MS Data. The column temperature was 25 °C, the flow rate was 0.3 mL/min, the injection volume was 2 μL, and the post-equilibrium time was 3 min. The composition of the mobile phase, the flow rate, and the column temperature were optimized for better resolution. Finally, (A) deionized water containing 0.1% formic acid and (B) acetonitrile were chosen as the mobile phase. The gradient

of the mobile phase was 0−4.5 min, 95% B; 4.5−6.0 min, 40.0−95% B; 6−17 min, 25−40% B; 17−19 min, 5−25% B.

The ionization modes detected by positive and negative ions of the electrospray ion source were as follows: a positive ion mode collision energy voltage of 30 V and a negative ion mode collision energy voltage of 35 V. The atomization gas was high purity nitrogen (N_2), and the collision gas was high-purity helium (He). The scanning range was 80−1200 m/z, the sheath pressure was 40 arb, the auxiliary pressure was 5 arb, the spray voltage was 3.0 kV, the ion transport tube temperature was 300 °C, the auxiliary gas heating temperature was 320 °C, the lens voltage was 50 V, and the resolution was 70,000 (primary mass spectrometry) 17,500 (secondary mass spectrometry) high energy collision dissociation.

4.6. Statistical Analysis. Raw data were processed with the Compound Discoverer 3.1 software (Thermo Scientific) for baseline filtering, peak identification, the peak extraction, integration, correction of retention time, peak alignment, combined ion merging, missing value filling, and peak area correction. Data processing for ESI⁺ and ESI⁻ was performed separately. Thresholds for peak detection included a minimum of six data points per peak. Metabolites were scored against the Human Metabolome Database (https://hmdb.ca/) spectra from the mzCloud database (www.mzcloud.org). For stability study data analysis, QC samples were analyzed to determine the extent of retention time variability and verify consistent mass accuracy throughout the analysis. The quality control samples with a relative standard deviation for peak area was 30%, and the signal-to-noise ratio (S/N) threshold was 3.

Data were exported from the UHPLC-MS/MS into SIMCA-P 13.0. PCA and PLS-DA were used to differentiate the samples. PCA scores were unsupervised as a basis for PLS-DA which was supervised. R_2 and Q_2 provided a measure of model reliability of PCA and PLS-DA.[54] The PLS-DA model was assessed by the intercepts of R_2 and Q_2 in the permutation test to avoid overfitting. The criteria for model validity included two conditions: (1) all Q_2 values on the permuted data set to the left were lower than the Q_2 values on the actual data set to the right and (2) the regression line (line joining the point of observed Q_2 to the centroid of a cluster of permuted Q_2 values) has a negative value of intercept on the y-axis.[55] Through the variable importance for the projection (VIP) of the PLS-DA model, the potential biomarker was found with VIP > 1. A larger VIP indicated a more important biomarker.

Data processing of each software package yielded a multidimensional peak table including accurate m/z, molecular weights, retention times, compound formulas, peak areas, and other statistical information. The differential metabolites with statistical significance were screened according to the difference multiple (fold change, FC) FC > 1.5 or FC < 0.67 and t-test (test level α = 0.05). In this study, compounds with VIP > 1, P < 0.05, and FC > 1.5 or FC < 0.67 were considered as differential metabolites.

4.7. Network Pharmacology Analysis. The PubChem (https://pubchem.ncbi.nlm.nih.gov/) database was used to retrieve artesunate 3D/2D structure information, SMILES, and CID numbers. The putative targets of artesunate were obtained from the online prediction platforms of SwissTarget-Prediction (http://swisstargetprediction.ch/), Charit.ed - About SuperPred (https://prediction.charite.de/), PharmMapper (http://lilab-ecust.cn/pharmmapper/index.html), and published literature studies. All the retrieved targets were

converted to their official symbols using the Uniprot (https://www.uniprot.org/).

The malaria-related target proteins were collected from GeneCard (https://www.genecards.org/). This was a comprehensive database of human genes and covered the analytical data of genes in multiple databases.[56] By intersecting the putative target genes of artesunate with malaria-related target proteins, genes that correspond simultaneously to disease and treatment were considered potential targets of artesunate.

GO enrichment and KEGG pathway enrichment analyses were undertaken to probe the biological function and potential mechanisms of detected targets (https://david.ncifcrf.gov/). Meanwhile, the acquired target genes were submitted to the Search Tool for the Retrieval of Interacting Genes (https://www.stringdb.org/) to obtain a protein–protein interaction network.[57] Furthermore, a compound–potential targets–potential pathways network of artesunate for treating malaria was constructed by utilizing the network-visualization software Cytoscape 3.7.1 (http://cytoscape.org/).

■ AUTHOR INFORMATION

Corresponding Authors

Qiuhong Zhang − *Jinan Center for Food and Drug Control, Jinan 250102, P. R. China*; Email: zhangqh9886@163.com

Huimin Zhang − *Shandong Academy of Chinese Medicine, Jinan 250014, P. R. China*; Email: huiminzhang@163.com

Authors

Feiran Wang − *Shandong University of Traditional Chinese Medicine, Jinan 250355, P. R. China; Shandong Academy of Chinese Medicine, Jinan 250014, P. R. China*; orcid.org/0000-0002-3785-2632

Jian Song − *Shandong University of Traditional Chinese Medicine, Jinan 250355, P. R. China*

Yingying Yan − *Shandong University of Traditional Chinese Medicine, Jinan 250355, P. R. China*

Qian Zhou − *Shandong Academy of Chinese Medicine, Jinan 250014, P. R. China*

Xiaojing Li − *Shandong Academy of Chinese Medicine, Jinan 250014, P. R. China*

Ping Wang − *Shandong Academy of Chinese Medicine, Jinan 250014, P. R. China*

Zongtong Yang − *Shandong Academy of Chinese Medicine, Jinan 250014, P. R. China*

Complete contact information is available at:
https://pubs.acs.org/10.1021/acsomega.2c04157

Author Contributions

‖F.W. and J.S. contributed equally.

Notes

The authors declare no competing financial interest.

■ ACKNOWLEDGMENTS

■ ABBREVIATIONS

Hal, histidine ammonia-lyase; Amdhd1, probable imidazolonepropionase; Fah, fumarylacetoacetate hydrolase; Odc1, ornithine decarboxylase; Sms, spermine synthase; Sat1, diamine acetyltransferase 1; UCK2 tetramer, uridine-cytidine kinase 2; CK, choline kinase; Chdh, choline dehydrogenase, mitochondrial; CCT, CTP, phosphocholine cytidylyltransferase; Aldh7a1, alpha-aminoadipic semialdehyde dehydrogenase A; CEPT, choline/ethanolaminephosphotransferase; ART, aryl hydrocarbon receptor; ChAT, choline acetyl transferase

■ REFERENCES

(1) World Health, O. *World Malaria Report 2021*; World Health Organization: Geneva, 2021; pp 9−21.

(2) Winzeler, E. A. Malaria research in the post-genomic era. *Nature* **2008**, *455*, 751−756.

(3) Blackman, M. J.; Carruthers, V. B. Recent insights into apicomplexan parasite egress provide new views to a kill. *Curr. Opin. Microbiol.* **2013**, *16*, 459−464.

(4) Nicole, K.; Jae-Yeon, C.; Dennis, R. V.; Choukri, B. M. Role of phospholipid synthesis in the development and differentiation of malaria parasites in the blood. *J. Biol. Chem.* **2018**, *293*, 17308−17316.

(5) Cowman, A. F.; Healer, J.; Marapana, D.; Marsh, K. Malaria: Biology and Disease. *Cell* **2016**, *167*, 610−624.

(6) Kasturi, H.; Narla, M. Malaria, erythrocytic infection, and anemia. *Hematology. Am. Soc. Hematol. Educ Program.* **2009**, *2009*, 87−93.

(7) Podgorski, R. M.; Goff, K. A.; Penney, T. P.; Maness, N. J.; Keating, J.; Yukich, J. O.; Marx, P. A. DNA analysis reveals non-falciparum malaria in the Democratic Republic of the Congo. *Acta Trop.* **2020**, *212*, 105557.

(8) Wykes, M. N.; Good, M. F. What have we learnt from mouse models for the study of malaria? *Eur. J. Immunol.* **2009**, *39*, 2004−2007.

(9) Wang, J. G.; Xu, C. C.; Wong, Y. K.; Li, Y. J.; Liao, F. L.; Jiang, T. L.; Tu, Y. Y. Artemisinin, the Magic Drug Discovered from Traditional Chinese Medicine. *Engineering* **2019**, *5*, 32−39.

(10) Bai, X. Y.; Liu, P.; Chai, Y. W.; Wang, Y.; Ren, S. H.; Li, Y. Y.; Zhou, H. Artesunate attenuates 2, 4-dinitrochlorobenzene-induced atopic dermatitis by down-regulating Th17 cell responses in BALB/c mice. *Eur. J. Pharmacol.* **2020**, *874*, 173020.

(11) Dai, Y. F.; Zhou, W. W.; Meng, J.; Du, X. L.; Sui, Y. P.; Dai, L.; Wang, P. Q.; Huo, H. R.; Sui, F. The pharmacological activities and mechanisms of artemisinin and its derivatives: a systematic review. *Med. Chem. Res.* **2017**, *26*, 867−880.

(12) Li, S.; Li, C. H.; Jiang, T. L. [Reasearch on lipid metabolism of Plasmodium and antimalarial mechanism of artemisinin]. *Zhongguo Zhongyao Zazhi* **2021**, *46*, 4849−4864.

(13) Wang, J. G.; Zhang, C. J.; Chia, W. N.; Loh, C. C. Y.; Li, Z. J.; Lee, Y. M.; He, Y.; Yuan, L. X.; Lim, T. K.; et al. Haem-activated promiscuous targeting of artemisinin in Plasmodium falciparum. *Nat. Commun.* **2015**, *6*, 10111.

(14) Hartwig, C. L.; Rosenthal, A. S.; D'Angelo, J.; Griffin, C. E.; Posner, G. H.; Cooper, R. A. Accumulation of artemisinin trioxane derivatives within neutral lipids of Plasmodium falciparum malaria parasites is endoperoxide-dependent. *Biochem. Pharmacol.* **2009**, *77*, 322−336.

(15) Wang, J.; Huang, L.; Li, J.; Fan, Q. W.; Long, Y. C.; Li, Y.; Zhou, B. Artemisinin directly targets malarial mitochondria through its specific mitochondrial activation. *PLoS One* **2010**, *5*, No. e9582.

(16) Krishna, S.; Uhlemann, A. C.; Haynes, R. K. Artemisinins: mechanisms of action and potential for resistance. *Drug Resistance Updates* **2004**, *7*, 233−244.

(17) Wang, W. B.; Zhao, L. L.; He, Z. Y.; Wu, N.; Li, Q. X.; Qiu, X. J.; Zhou, L.; Wang, D. S. Metabolomics-based evidence of the hypoglycemic effect of Ge-Gen-Jiao-Tai-Wan in type 2 diabetic rats

via UHPLC-QTOF/MS analysis. *J. Ethnopharmacol.* **2018**, *219*, 299−318.

(18) Chora, Â. F.; Mota, M. M.; Miguel, P. The reciprocal influence of the liver and blood stages of the malaria parasite's life cycle. *Int. J. Parasitol.* **2022**, *30*, 00054−00056.

(19) Ishino, T.; Yano, K.; Chinzei, Y.; Yuda, M. Cell-Passage Activity Is Required for the Malarial Parasite to Cross the Liver Sinusoidal Cell Layer. *PLoS Biol.* **2004**, *2*, No. e4.

(20) Bhanot, P.; Schauer, K.; Coppens, I.; Nussenzweig, V. A Surface Phospholipase Is Involved in the Migration of Plasmodium Sporozoites through Cells. *J. Biol. Chem.* **2005**, *280*, 6752−6760.

(21) Risco-Castillo, V.; Topçu, S.; Marinach, C.; Manzoni, G.; Bigorgne, A. E.; Briquet, S.; Baudin, X.; Lebrun, M.; Dubremetz, J. F.; Silvie, O. Malaria Sporozoites Traverse Host Cells within Transient Vacuoles. *Cell Host Microbe* **2015**, *18*, 593−603.

(22) Al-Dhalimy, M.; Overturf, K.; Finegold, M.; Grompe, M. Long-Term Therapy with NTBC and Tyrosine-Restricted Diet in a Murine Model of Hereditary Tyrosinemia Type I. *Mol. Genet. Metab.* **2002**, *75*, 38−45.

(23) Cyr, A.; Lauryn, K.; Lauran, C.; Sladjana, S.; Brian, Z.; Cristina, A. Circulating Metabolomic Analysis following Cecal Ligation and Puncture in Young and Aged Mice Reveals Age-Associated Temporal Shifts in Nicotinamide and Histidine/Histamine Metabolic Pathways. *Oxid. Med. Cell. Longevity* **2021**, *2021*, 5534241.

(24) Swaminathan, M.; Hill-Yardin, E. L.; Bornstein, J. C.; Foong, J. P. P. Endogenous Glutamate Excites Myenteric Calbindin Neurons by Activating Group I Metabotropic Glutamate Receptors in the Mouse Colon. *Front. Neurosci.* **2019**, *13*, 00426.

(25) Misselbeck, K.; Marchetti, L.; Priami, C.; Stover, P. J.; Field, M. S. The 5-formyltetrahydrofolate futile cycle reduces pathway stochasticity in an extended hybrid-stochastic model of folate-mediated one-carbon metabolism. *Sci. Rep.* **2019**, *9*, 4322.

(26) Yan, Y. L.; Yan, Q. J.; Qian, L.; Jiang, Y. P.; Chen, X.; Zeng, S. S.; Xu, Z. J.; Gong, Z. C. S-adenosylmethionine administration inhibits levodopa-induced vascular endothelial growth factor-A expression. *Aging* **2020**, *12*, 21290−21307.

(27) Geditz, M. C. K.; Heinkele, G.; Ahmed, A.; Kremsner, P. G.; Kerb, M. S.; Schwab, M.; Hofmann, U. LC-MS/MS method for the simultaneous quantification of artesunate and its metabolites dihydroartemisinin and dihydroartemisinin glucuronide in human plasma. *Anal. Bioanal. Chem.* **2014**, *406*, 4299−4308.

(28) Li, N.; Sun, W. J.; Zhou, X.; Gong, H.; Chen, Y. Q.; Chen, D. F.; Xiang, F. Dihydroartemisinin Protects against Dextran Sulfate Sodium-Induced Colitis in Mice through Inhibiting the PI3K/AKT and NF-κB Signaling Pathways. *BioMed Res. Int.* **2019**, *2019*, 1415809.

(29) Ou, L.; Qin, K.; Yang, Z. X.; Bie, M. J. The Effects and Mechanisms of Dihydroartemisinin on Influenza A Virus H1N1 Induces TNF-α and IL-6 Expression in Bronchial Epithelial Cells. *Sichuan Daxue Xuebao, Yixueban* **2020**, *51*, 171−177.

(30) Cetrullo, S.; D'Adamo, S.; Tantini, B.; Borzi, R. M.; Flamigni, F. mTOR, AMPK, and Sirt1: Key Players in Metabolic Stress Management. *Crit. Rev. Eukaryotic Gene Expression* **2015**, *25*, 59−75.

(31) Zhang, Z. L.; Guo, M.; Zhao, S. F.; Shao, J. J.; Zheng, S. Z. ROS-JNK1/2-dependent activation of autophagy is required for the induction of anti-inflammatory effect of dihydroartemisinin in liver fibrosis. *Free Radical Biol. Med.* **2016**, *101*, 272−283.

(32) Gu, D. D.; Nan, Q.; Miao, Y. L.; Yang, H. L.; Li, M. J.; Ye, Y.; Miao, J. R. KT2 alleviates ulcerative colitis by reducing Th17 cell differentiation through the miR-302c-5p/STAT3 axis. *Eur. J. Cell Biol.* **2022**, *101*, 151223.

(33) Aoki, R.; Ayako, A. Y.; Chise, S.; Yoshiharu, T. Indole-3-Pyruvic Acid, an Aryl Hydrocarbon Receptor Activator, Suppresses Experimental Colitis in Mice. *J. Immunol.* **2018**, *201*, 3683−3693.

(34) Xie, J. M.; Wang, Z. T.; Wang, W. Semaphorin 4D Induces an Imbalance of Th17/Treg Cells by Activating the Aryl Hydrocarbon Receptor in Ankylosing Spondylitis. *Front. Immunol.* **2020**, *11*, 2151.

(35) Keswani, T.; Bhattacharyya, A. Differential role of T regulatory and Th17 in Swiss mice infected with Plasmodium berghei ANKA and Plasmodium yoelii. *Exp. Parasitol.* **2014**, *141*, 82−92.

(36) Bannister, L. H.; Hopkins, J. M.; Fowler, R. E.; Krishna, S.; Mitchell, G. H. A Brief Illustrated Guide to the Ultrastructure of Plasmodium falciparum Asexual Blood Stages. *Parasitol. Today* **2000**, *16*, 427−433.

(37) Flammersfeld, A.; Lang, C.; Flieger, A.; Pradel, G. Phospholipases during membrane dynamics in malaria parasites. *Int. J. Med. Microbiol.* **2018**, *308*, 129−141.

(38) Pessi, G.; Guillermo, K.; Choukri, B. M. A pathway for phosphatidylcholine biosynthesis in Plasmodium falciparum involving phosphoethanolamine methylation. *Proc. Natl. Acad. Sci. U.S.A.* **2004**, *101*, 6206−6211.

(39) Miller, L. H.; Ackerman, H. C.; Su, X. Z.; Wellems, T. E. Malaria biology and disease pathogenesis: insights for new treatments. *Nat. Med.* **2013**, *19*, 156−167.

(40) Tran, P. N.; Brown, S. H. J.; Rug, M.; Ridgway, M. C.; Mitchell, T. W.; Maier, A. G. Changes in lipid composition during sexual development of the malaria parasite Plasmodium falciparum. *Malar. J.* **2016**, *15*, 73.

(41) Déchamps, S.; Wengelnik, K.; Berry-Sterkers, L.; Cerdan, R.; Vial, H. J.; Gannoun-Zaki, L. The Kennedy phospholipid biosynthesis pathways are refractory to genetic disruption in Plasmodium berghei and therefore appear essential in blood stages. *Mol. Biochem. Parasitol.* **2010**, *173*, 69−80.

(42) Ancelin, M. L.; Parant, M.; Thuet, M. J.; Philippot, J. R.; Vial, H. J. Increased permeability to choline in simian erythrocytes after Plasmodium knowlesi infection. *Biochem. J.* **1991**, *273*, 701−709.

(43) Sibmooh, N.; Pipitaporn, B.; Wilairatana, P.; Dangdoungjai, J.; Udomsangpetch, R.; Looareesuwan, S.; Chantharaksri, U. Effect of Artemisinin on Lipid Peroxidation and Fluidity of the Erythrocyte Membrane in Malaria. *Biol. Pharm. Bull.* **2000**, *23*, 1275−1280.

(44) Maruyama, T.; Asuka, M.; Toshiyuki, I.; Yoshihiko, K.; Makoto, K. P2X2 receptors supply extracellular choline as a substrate for acetylcholine synthesis. *FEBS Open Bio* **2021**, *12*, 250−257.

(45) Jarczyk, J.; Benito, A. Y.; Simone, H. The Cholinergic Anti-Inflammatory Pathway as a Conceptual Framework to Treat Inflammation-Mediated Renal Injury. *Kidney Blood Pressure Res.* **2019**, *44*, 435−448.

(46) Inoue, T.; Tanaka, S.; Okusa, M. D. Neuroimmune Interactions in Inflammation and Acute Kidney Injury. *Front. Immunol.* **2017**, *8*, 945.

(47) Nullens, S.; Staessens, M.; Peleman, C.; Schrijvers, D. M.; Malhotra-Kumar, S.; Francque, S.; Matteoli, G.; Boeckxstaens, G. E.; De Man, J. G. D.; De Winter, B. Y. D. Effect of Gts-21, An Alpha7 Nicotinic Acetylcholine Receptor Agonist, on Clp-Induced Inflammatory, Gastrointestinal Motility, and Colonic Permeability Changes in Mice. *Shock* **2016**, *45*, 450−459.

(48) Bando, H.; Pradipta, A.; Iwanaga, S.; Okamoto, T.; Okuzaki, D.; Tanaka, S.; Vega-Rodríguez, J.; Lee, Y.; Ma, J. S.; Sakaguchi, N.; et al. CXCR4 regulates Plasmodium development in mouse and human hepatocytes. *J. Exp. Med.* **2019**, *216*, 1733−1748.

(49) Jiang, Y.; Du, H. J.; Liu, X.; Fu, X.; Li, X. D.; Cao, Q. Artemisinin alleviates atherosclerotic lesion by reducing macrophage inflammation via regulation of AMPK/NF-κB/NLRP3 inflammasomes pathway. *J. Drug Targeting* **2020**, *28*, 70−79.

(50) Hsiao, L. L.; Howard, R. J.; Aikawa, M.; Taraschi, T. F. Modification of host cell membrane lipid composition by the intra-erythrocytic human malaria parasite Plasmodium falciparum. *Biochem. J.* **1991**, *274*, 121−132.

(51) Parsel, S. M.; Gustafson, S. A.; Friedlander, E.; Shnyra, A. A.; Adegbulu, A. J.; Liu, Y.; Parrish, N. M.; Jamal, S. A.; Lofthus, E.; Ayuk, L.; et al. Malaria over-diagnosis in Cameroon: diagnostic accuracy of Fluorescence and Staining Technologies (FAST) Malaria Stain and LED microscopy versus Giemsa and bright field microscopy validated by polymerase chain reaction. *Infect. Dis. Poverty* **2017**, *6*, 32−40.

(52) Sitali, L.; Miller, J. M.; Mwenda, M. C.; Bridges, D. J.; Hawela, M. B.; Hamainza, B.; Chizema-Kawesha, E.; Eisele, T. P.; Chipeta, J.;

Lindtjørn, B. Distribution of Plasmodium species and assessment of performance of diagnostic tools used during a malaria survey in Southern and Western Provinces of Zambia. *Malar. J.* **2019**, *18*, 130−139.

(53) Wei, H.; Jin, C. X.; Peng, A. P.; Xie, H. Y.; Xie, S. H.; Feng, Y. F.; Xie, A. Q.; Li, J. J.; Fang, C.; Yang, Q.; et al. Characterization of $\gamma\delta$T cells in lung of Plasmodium yoelii-infected C57BL/6 mice. *Malar. J.* **2021**, *20*, 89−104.

(54) Yang, C. M.; Guang, P. W.; Li, L.; Song, H.; Huang, J.; Li, Y.; Wang, L.; Hu, J. Early rapid diagnosis of Alzheimer's disease based on fusion of near- and mid-infrared spectral features combined with PLS-DA. *Optik* **2021**, *241*, 166485.

(55) Mahadevan, S.; Shah, S. L.; Marrie, J. M.; Slupsky, C. M. Analysis of Metabolomic Data Using Support Vector Machines. *Anal. Chem.* **2008**, *80*, 7562−7570.

(56) Stelzer, G.; Rosen, N.; Plaschkes, I.; Zimmerman, S.; Twik, M.; Fishilevich, S.; Stein, T. I.; Nudel, R.; Lieder, I.; Mazor, Y..; et al. The GeneCards Suite: From Gene Data Mining to Disease Genome Sequence Analyses. *Curr. Protoc. Bioinf.* **2016**, *54*, 1.30.1.

(57) Szklarczyk, D.; Andrea, F.; Stefan, W.; Kristoffer, F.; Davide, H.; Jaime, H. C.; Milan, S.; Alexander, R.; Alberto, S.; Tsafou, K. P.; et al. STRING v10: protein−protein interaction networks, integrated over the tree of life. *Nucleic Acids Res.* **2015**, *43*, D447−D452.